LAWRENCE
LIVERMORE
NATIONAL
LABORATORY

UCRL-JRNL-225816

Very-high-growth-factor Planar Ablative Rayleigh Taylor Experiments

D. K. Bradley, D. G. Braun, S. G. Glendinning, M. J. Edwards, J. L. Milovich, C. M. Sorce, G. W. Collins, S. W. Haan, R. H. Page

November 3, 2006

Physics of Plasmas

Very-high-growth-factor Planar Ablative Rayleigh Taylor Experiments

D. K. Bradley, D. G. Braun, S. G. Glendinning, M. J. Edwards, J. L. Milovich, C. M. Sorce, G. W. Collins, S. W. Haan, R. H. Page

Lawrence Livermore National Laboratory,
P. O. Box 808,
Livermore CA 94550

Abstract

The Rayleigh-Taylor (RT) instability is an important factor in bounding the performance envelope of ignition targets. This paper describes an experiment for ablative RT instability that for the first time achieves growth factors close to those expected to occur in ignition targets at the National Ignition Facility (NIF). The large growth allows small-seed perturbations to be detected and can be used to place an upper bound on perturbation growth at the ablation front resulting from microstructure in the preferred Be ablator. The experiments were performed on the Omega laser using a halfraum 1.2 mm long by 2 mm diameter with a 75% laser entrance hole. The halfraum was filled with ~ 1 atm of neopentane to delay gold plasma from closing the diagnostic line of sight down the axis of the halfraum. The ablator was mounted at the base of the halfraum, and was accelerated by a two stepped X-ray pulse consisting of an early time section ~ 100 eV to emulate the NIF foot followed by an approximately constant ~ 150 eV drive sustained over an additional 5-7ns. It is this long pulse duration and late time observation that distinguishes the present work from previous experiments, and is responsible for the large growth that is achieved. The growth of a 2D sinusoidal perturbation machined on the drive side of the ablator was measured using face-on radiography. The diagnostic view remained open until ~ 11 ns with maximum growth factors measured to be ~ 200. The trajectory of the ablator was measured using streaked backlit radiography. The design and analysis of the experiments is described, and implications for experiments on ignition target ablators are discussed.

Introduction

Control and understanding of hydrodynamic instability growth is vital for the success of inertial confinement fusion (ICF) [1]. For ignition to occur, a capsule consisting of a low-z ablator material surrounding a layer of fusion fuel (typically DT) is imploded such that the fuel is compressed to ~1000mg/cm^2. The implosion is driven by ablation of the outer layer of the capsule. During the initial part of the implosion, as the capsule is accelerated inwards, the ablation front is hydrodynamically unstable and small perturbations, seeded by surface roughness or target imperfections, can grow via the Rayleigh-Taylor instability (RTI) [2, 3]. Although the instability is strongly stabilized by ablation and density gradients, growth factors ~ 100 are typical for modes <~ 50-100 by the time the capsule reaches peak velocity. During the same period, the DT ice ablator

interface is also susceptible to RTI. The seed for the instability comes from both surface roughness and velocity perturbations imposed on the shock waves as they traverse structure such as voids in the ablator. While growth at this interface is stabilized at high modes >~1000 by a sharp density gradient, growth factors ~1000 are typical. If the combined effect of this growth is large enough, these perturbations can break up the shell in flight, preventing both efficient compression of the fuel and ignition. If this does not happen, the perturbations can still feed through to the inside surface of the DT ice , where they grow due to RTI on deceleration. If they become too large, the energy of the implosion is not adequate to heat the hot spot to the temperature required for ignition For a successful implosion it is therefore important to minimize both the seeds and the total instability growth

Beryllium is the preferred capsule ablator material[4] for ignition experiments on the National Ignition Facility (NIF) [5, 6] for a number of reasons. It is a very efficient ablator, with a low albedo, and thus offers the potential for successful ignition with much lower drive temperatures (~250eV), [7] than other candidate materials such as plastic (CH). Its high tensile strength allows capsules to be filled with fuel at room temperature, and its high thermal conductivity helps in making the DT ice surface smooth in low modes[8]. Additionally its high density and high mass ablation rate makes it very tolerant of hydrodynamic instabilities[9]. The NIF point design capsule uses several sputtered Be layers in the ablator, each with a different amount of Cu-doping, ranging from 0-0.7%. [4] This design further reduces the potential for unstable growth by optimizing ablation rate and the density profile during the implosion.

The seeds for unstable growth are controlled by tight specifications on allowable roughness, as a function of mode number, for all surfaces and interfaces of the ablator and for the cryogenic DT layer. The allowable surface roughness for Be is 2-3x that of a comparable CH capsule. However, other potential seeds exist. Be is an anisotropic crystalline material with grain structure, and it may also have voids. It is possible that anisotropic wave speeds in solid crystals could act as a seed for instability as shocks pass through it. This effect is minimized in the point design by ensuring that the first shock that passes through the Be has sufficient pressure to melt it. Target fabrication techniques have also been refined to produce coatings with uniform microstructure and void volumes that meet tight tolerance specifications. As an additional verification an experimental program has been developed to quantify the effects of microstructure and surface finish.

Since an imploding ignition capsule can undergo large amounts of unstable growth between the start of acceleration and peak compression (factors ~1000x are typical) the allowable seeds are very small (typically ~20 nm at the capsule surface, or <1 part in 10^4 in shock uniformity) and hence very difficult to detect. One technique is to allow the initial perturbation to grow through RT amplification to a level at which it can be measured and diagnosed. However, even with sensitive diagnostics this requires growth factors that are comparable to those expected on NIF and are many times higher than those previously achieved[9-12].

In this paper we discuss the development of a very high growth factor RT platform that has produced growth factors (GF's) up to 200X for 200 nm peak-to-valley perturbations in Br-doped CH. The development shots have been carried out using a single wavelength perturbation on planar plastic foils for ease of manufacture and

diagnostic sensitivity. A scaling of our results indicates that we should be able to detect the effects of perturbations comparable to 1-3x the NIF capsule surface specifications (~20-60 nm rms) in 3% Cu-doped Be

Experiment

The experiments were designed using a series of 2 D simulations with the radiation hydrodynamics code Lasnex [13]. The goal was to try to optimize the amount of unstable growth in the package while maintaining a clear line of sight for face-on radiography. This required balancing the need for a large diameter hohlraum, to delay plasma filling of the line-of-sight, with the need for a high radiation temperature, which would require a small volume. The radiation drive was produced by an Omega-scale-1 (i.e. radius=800 μm) half-hohlraum, or halfraum, 1 mm in length. The length was chosen to optimize the drive temperature, without causing the beams to hit the package. Additionally the halfraum was filled with 1 atmosphere of neopentane to delay filling.

Experiments were conducted using the 60 beam OMEGA laser system[14] at the University of Rochester. The longest pulse duration currently available on OMEGA is 3.8 ns, with energy falling for the longer pulse lengths, so the long-duration drive for our experiment was achieved by staggering a series of shorter-pulse beams in time. Two drive-beam configurations were used for these experiments: one with hexagonal azimuthal symmetry; and one with pentagonal symmetry. For the hexagonal case, the OMEGA beams are incident at the LEH in a series of cones: 6 beams at 23 degrees, 6 at 48 degrees, 3 at 59 degrees and 6 at 62 degrees. Our drive was constructed of symmetrical (minimum of three at any given time) subsets of those cones, staggered in time, as shown in figure 1. The pulse shape used to build the drive was a ~2.4 ns duration reverse-ramp with a maximum energy of 350 J/beam. For the pentagonal case, the beams are incident in cones of 5 beams at 21 degrees, 5 beams at 42 degrees, and 10 beams at 58 degrees. The drive used in that geometry was constructed using full cones in 3 temporal sequences as shown in figure 2. This configuration was designed to optimize azimuthal symmetry. The predicted radiation drives for both geometries are also shown in figs 1 and 2. In each case the drive consists of a low temperature, ~100eV "foot" that is designed to compress the foil with the longer, higher temperature, part of the drive providing the acceleration. The radiation temperature (T_r) in the foot can be adjusted to closely match conditions in the early part of the NIF ignition drive.

Samples for the platform verification experiments consisted of 4% Br-doped polystyrene (CH) foils with a wavelength $\lambda = 50$ μm sinusoidal perturbation machined on one side. The foils were mounted on a series of half-hohlraums (halfraums) 1800 μm diameter, 1000 μm length, with 1200 μm laser entrance holes (LEH's). In each case the foils were mounted on a 900 μm hole opposing the LEH with the rippled side pointing towards the interior of the halfraum. The LEH was covered by a 400 nm polyimide window which allowed the halfraum to be filled with 1 atm. neopentane to prevent early filling of the line of sight with gold plasma.

The gas-fill is vital to the success of the experiment. Figure 3 shows the results of 2-dimensional simulations of the platform for the case of a vacuum halfraum , and one filled with 3.0 mg/cc (1 atmosphere) C_5H_{12}. At a time of 8 ns the vacuum case shows a

significant influx of gold towards the axis of the halfraum. However, in the gas-filled halfraum the gold is still >325μm from the axis at the LEH. A plot of the optical depth of the halfraum to 4keV x-ray radiation along a line 300μm from the axis shows very high absorption for the vacuum case (due to the gold), with an optical depth ~1.5 for the gas-fill. Fig 4 shows the predicted T_r for both cases. It is interesting to note that although the temperature towards the LEH is very similar, the temperature, and hence drive seen by the foil is very different in the two cases. This results in a significantly different displacement history, as seen in figure 4(b). The gas-fill case starts later because of the time needed to burn through the polyimide foil and the gas but then shows much greater acceleration throughout the drive.

The expected number of growth factors for a 40 μm 4% Br-doped CH foil a as a function of time is shown in fig 5 for a range of initial amplitude perturbations. The growth factor (GF) at time t is defined in the code as

$$GF = \{RMS\ (\int \rho dz)]_t\ / [RMS(\int \rho dz)\}_{t=0}$$

where ρ is the foil density and z is the direction along the halfraum axis. As expected, all the amplitudes show similar growth early in time. The larger initial amplitudes stop growing earlier due to non-linear saturation and foil burn through. The smallest perturbation (similar to levels in the NIF surface roughness specification) continues to grow, up to a factor >1000x by 12 ns. The corresponding saturation amplitudes are similar in each case (with adjustments made for ablation). Thinner foils will accelerate more, and hence grow more quickly, but will burn through earlier, whereas thicker foils can support more growth but will grow more slowly. It is important therefore to optimize the foil thickness and the viewing time. The experiments reported in this paper used 40-65 μm thick foils with initial perturbations ranging from 200nm to 1000nm peak-to-valley (P-V). A 50 μm wavelength was chosen for the experiments because it lies at the peak of the RT dispersion curve for Be and is close to the most damaging mode in the ignition capsule[15].

Figure 6 shows a schematic of the experimental setup. A backlighter foil consisting of 12.5 μm Sc and 125μm Be was mounted 1.5 mm from the package. Face-on radiography of the accelerated foils was carried out by illuminating the Sc foil with up to 13 OMEGA beams, time staggered to give an aprrox 0.8 TW, 4.5 ns duration pulse with little temporal modulation. A spatially uniform backlighter profile was achieved by using distributed phase plates (DPP's) producing a supergaussian spatial distribution with a ~650μm central region of uniform intensity. The Be foil prevented the Sc backlighter from exploding, or accelerating towards the package during the experiment. An imaging x-ray framing camera positioned at the LEH side of the halfraum recorded time resolved images of the backlighter x-rays viewed through the package with a magnification of 12x and a temporal resolution of 70-80 ps. The camera was filtered with a total of 275 μm Be, and 12.5 μm Sc (in addition to the self-filtering of the 12.5 μm Sc backlighter foil itself) so that the principal x-ray energy detected was the n=2-1 He-like Sc line at ~4.3 keV.

The trajectory of the accelerated foil was measured as a function of time on several shots using streaked radiography, as shown in figure 7. There was no diagnostic viewing angle perpendicular to the LEH, so for these shots the rear surface of the halfraum was tilted by 10.8 degrees. Calculations using a view-factor code indicated that this would cause no significant compromise to the acceleration of the foil. The side-on radiography

used a vanadium backlighter, positioned 4 mm from the halfraum axis, and an x-ray streak camera with a 20x magnification and a 10 μm imaging slit. The duration of the x-ray pulse was ~7 ns.

The radiation drive in the experiment was measured using the multi-channel x-ray diode array Dante[16, 17] which recorded the time and spectrally resolved flux from the LEH. The measured radiation temperatures are shown in fig 1 and fig 2 and agree very well with the predicted values. Measurements of backscattered SRS and SBS were taken from one of the beams in the main drive cone and were found to be very small (2-3% each)

Figure 8 shows a sequence of face-on radiographs taken between 8.5 and 11 ns (using the 10.5 ns version of the drive) from a foil with an initial perturbation of 1100 nm peak-to-valley. The final set of 3 drive beams (23 degrees to the halfraum axis) can be seen at the edges of the first 4 images. The drive beams turn off between 10 and 10.5 ns after which the only signal comes from the backlighter. There are clear ripples visible in all the images, with increasing contrast later in time. The clear-aperture along the line-of-sight is beginning to close by 11 ns with a 3 lobed structure typical of the azimuthal beam distribution used on this shot. However several wavelengths of modulation are still visible. Figure 9 shows the measured modulation as a function of time from a series of similar shots shots, expressed as a growth factor, for both large and small initial amplitude cases. The small initial amplitude foils exhibit much higher GF's (~160x), compared to the low initial amplitudes (40-50x), as expected.

The 7.5 ns drive shown in figure 1 was designed as an improvement to the platform. The greater number of beams (minimum of 5) incident at a given time provides better azimuthal symmetry and the temporal shape of the drive accelerates the foil over a greater distance in a shorter time. Fig 10 shows data from a 41 μm thick foil with an initial 200nm P-V perturbation accelerated using the improved drive. The radiograph at 8.5 ns shows very clear modulations and a clear-aperture in excess of 650 μm. Analyzed data from side-on streaked radiography of a similar foil is shown in fig 11(a), together with a simulated trajectory generated from an integrated 2-d calculation using the measured laser-beam power histories as an input. The plot shows the measured trajectory of the inflection point in the x-ray transmission of the rear side of the foil. .The simulation agrees very well with the experiment, for both the time at which the foil begins to move, and for the trajectory to 10 ns. Face-on radiograph data from a pair of shots is plotted in fig11 (b). The analysis shows measured growth factors approaching 200x at 8.5 ns. The simulated optical depth values are close to those measured, but predict a slightly earlier burnthrough of the foil than observed. The data is consistent with fig 5, which shows an even smaller initial perturbation will continue to grow further.
It is useful to try and determine how small a perturbation we can measure using this platform. Figure 12 shows the results of a 2-D simulation in which a random perturbation corresponding to modes a-z of the NIF capsule specification was applied to a 50 μm 3% Cu-doped Be foil which was then accelerated using the fig 1 drive. The resulting density perturbation at 11 ns after the start of the drive is shown in fig. 12 (b), and the optical depth modulation generated by post-processing the data with a scandium x-ray spectrum is shown in fig. 12 (c). Also shown in fig 12(c) is the measured experimental diagnostic noise level. The optical depths in the simulation are 9x the levels of the noise, suggesting that NIF-level perturbations should be readily observable at 11 ns.

Summary

We have described the development of an ablative RT platform that for the first time achieves growth factors close to those expected to occur in ignition targets at the National Ignition Facility (NIF). The large growth allows small-seed perturbations to be detected and can be used to place an upper bound on perturbation growth at the ablation front resulting from microstructure in the preferred Be ablator. The initial experiments have been carried out using single mode machined perturbations on Br-doped CH foils. We have shown that we can keep the diagnostic view open for as long as 11 ns and we have measured growth factors as high as 200x at 8.5 ns. The results indicate that the platform can generate GF's in Cu-doped Be foils that are high enough to detect perturbations resulting from surface roughness at the NIF specification.

This work was performed under the auspices of the U.S. Department of Energy by University of California, Lawrence Livermore National Laboratory under Contract W-7405-Eng-48.

Figure captions

Figure 1. (a) Laser power history for the drive with hexagonal symmetry. (b) Predicted (dotted) and measured (solid) radiation temperature as a function of time. The simulated values have been postprocessed to reproduce the view seen by the experimental diagnostic

Figure 2. (a) Laser power history for the drive with pentagonal symmetry, (b) predicted (dotted) and measured (solid) radiation temperature in the halfraum as a function of time.

Figure 3. (a) Plot of simulated material distribution in the halfraum 8 ns after the start of the drive. Upper half is with 1 atmosphere C_5H_{12} fill, lower is for vaccum. (b) Cumulative optical depth along a line 0.3 mm from the axis for both cases.

Figure 4. (a) Simulated radiation temperature in the halfraum as a function of position for the 2 cases in figure 3. (b) Predicted foil displacement as a function of time

Figure 5. Predicted growth factors as a function of time for a λ=50 μm perturbation in a 41μm thick 4% Br-doped foil for 3 different initial amplitudes. The data points shown are from figure 11.

Figure 6. Experimental set up for face-on radiography

Figure 7. Configuration used for streaked foil trajectory measurements.

Figure 8. Sequence of radiographs taken at 9.5, 10.5, & 11 ns. The pairs of radiographs at each time are ~100 ps apart.

Figure 9. Measured growth factor as a function of time for 4%Br-doped CH foils with two different initial perturbations

Figure 10. Face-on radiograph taken at 8.5 ns

Figure 11. (a) Measured and simulated foil trajectory (b) Measured (points) and simulated (line) optical depth vs time for a 41 μm thick 4%Br-doped CH foilaccelerated using the drive of fig 2.

Figure 12 Growth of a random initial perturbation at the NIF surface specification for modes x-y (a) initial perturbation, (b) density contours at 11 ns, (c) optical depth modulations (blue line) resulting from propagating 2.8 kev x-rays through (b). The red line is typical diagnostic noise .

[1] J. D. Lindl, P. Amendt, R. L. Berger, et al., Physics of Plasmas **11**, 339 (2004).

[2] S. Chandrasekhar, *Hydrodynamic and Hydromagnetic Stability* (Oxford University Press, London, 1968).

[3] G. Taylor, Proceedings of the Royal Society of London, Series A (Mathematical and Physical Sciences) **201**, 192 (1950).

[4] S. W. Haan, M. C. Herrmann, T. R. Dittrich, et al., Physics of Plasmas **12**, 56316 (2005).

[5] J. A. Paisner, J. D. Boyes, S. A. Kumpan, et al., Laser Focus World **30**, 75 (1994).

[6] J. A. Paisner, J. D. Boyes, S. A. Kumpan, et al., in *SPIE-Int. Soc. Opt. Eng. Proceedings of the SPIE - The International Society for Optical Engineering, vol.2633, 1995, pp. 2-12. USA.*

[7] G. L. Strobel, S. W. Haan, D. H. Munro, et al., Physics of Plasmas **11**, 4695 (2004).

[8] J. D. Moody, B. J. Kozioziemski, R. L. London, et al., Journal de Physique IV **133**, 863 (2006).

[9] M. M. Marinak, S. G. Glendinning, R. J. Wallace, et al., Physics of Plasmas **9**, 3567 (2002).

[10] J. A. Cobble, T. E. Tierney, N. M. Hoffman, et al., Physics of Plasmas **13**, 56304 (2006).

[11] B. A. Remington, S. W. Haan, S. G. Glendinning, et al., Physics of Fluids B (Plasma Physics) **4**, 967 (1992).

[12] S. V. Weber, B. A. Remington, S. W. Haan, et al., Physics of Plasmas **1**, 3652 (1994).

[13] reference for Lasnex

[14] T. R. Boehly, D. L. Brown, R. S. Craxton, et al., Optics Communications **133**, 495 (1997).

[15] need a reference for where damaging modes are

[16] H. N. Kornblum, R. L. Kauffman, and J. A. Smith, Review of Scientific Instruments **57**, 2179 (1986).

[17] K. M. Campbell, F. A. Weber, E. L. Dewald, et al., Review of Scientific Instruments **75**, 3768 (2004).

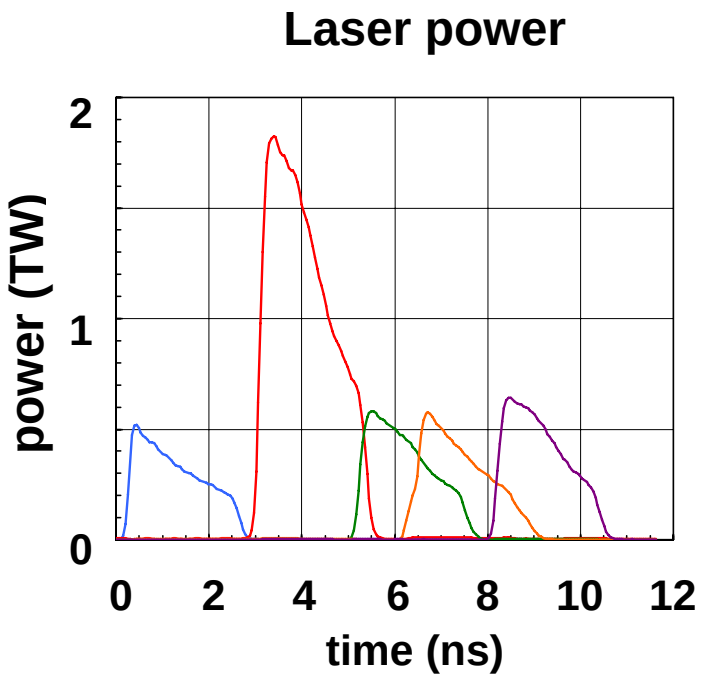
Laser power
power (TW)
2
1
0
0
2
4
6
8
10
12
time (ns)

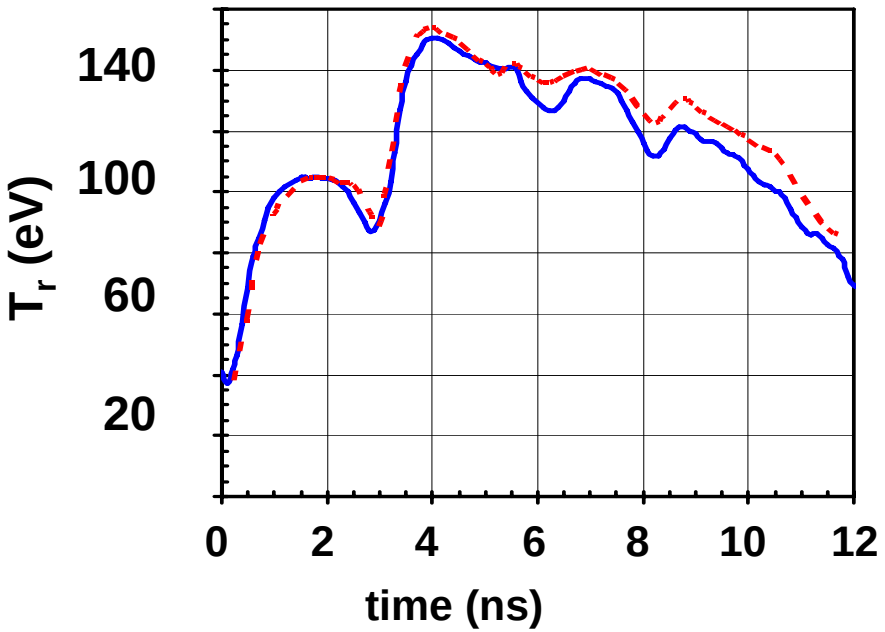
T_r (eV)
140
100
60
20
0
2
4
6
8
10
12
time (ns)

figure 1

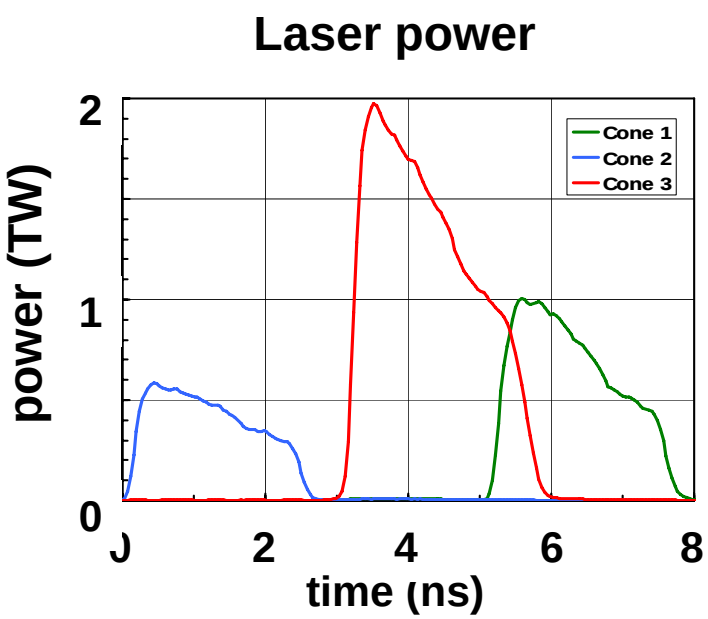
Laser power
power (TW)
2
1
0
0
2
4
6
8
time (ns)
Cone 1
Cone 2
Cone 3

(a)

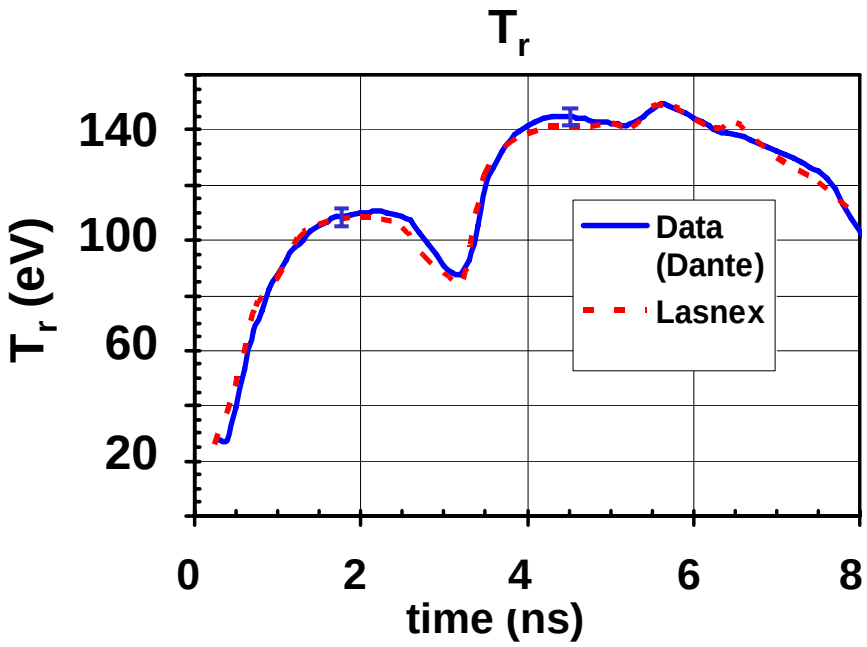
T_r
T_r (eV)
140
100
60
20
0
2
4
6
8
time (ns)
Data
(Dante)
Lasnex

(b)

Figure 2

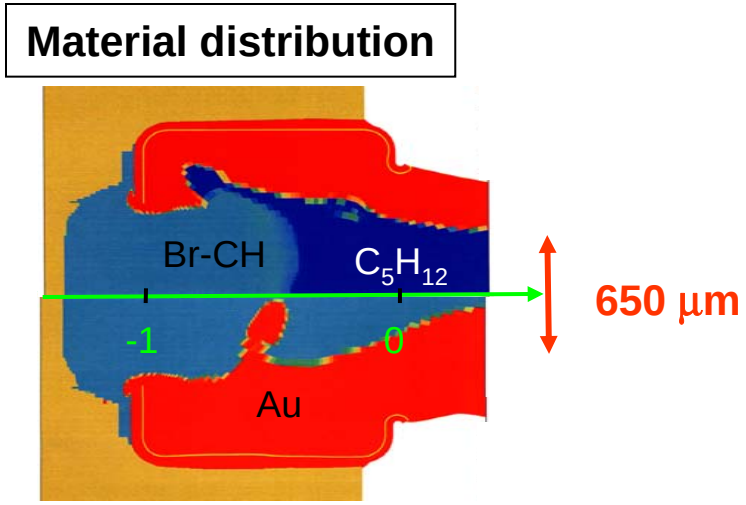
Material distribution
Br-CH
C_5H_{12}
650 μm
-1
0
Au

(a)

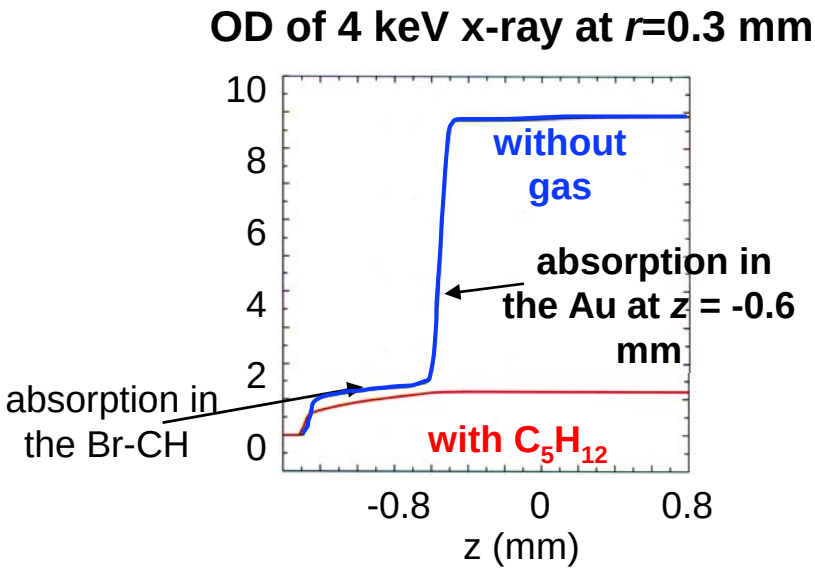
OD of 4 keV x-ray at r=0.3 mm
10
8
6
4
2
0
without gas
absorption in the Au at z = -0.6 mm
absorption in the Br-CH
with C_5H_{12}
-0.8
0
0.8
z (mm)

(b)

Fig 3

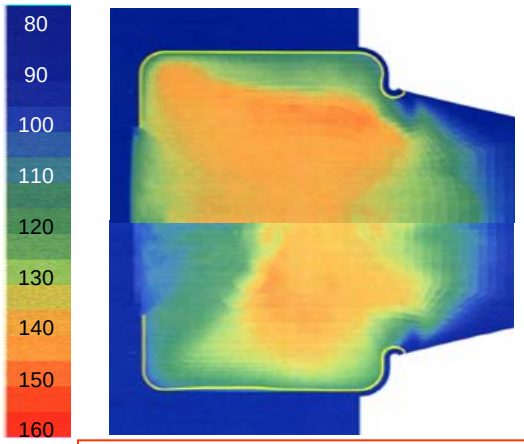
80
90
100
110
120
130
140
150
160
3.0 mg/cc
C_5H_{12} fill
no gas
fill
RadiationTemperature

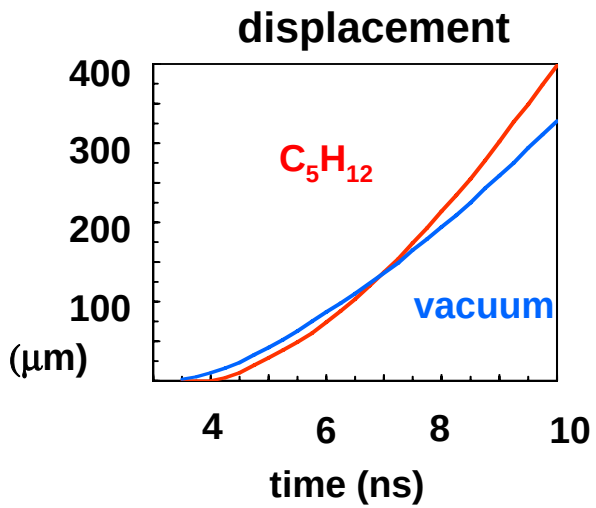
displacement
400
300
200
100
(μm)
C_5H_{12}
vacuum
4
6
8
10
time (ns)

Figure 4

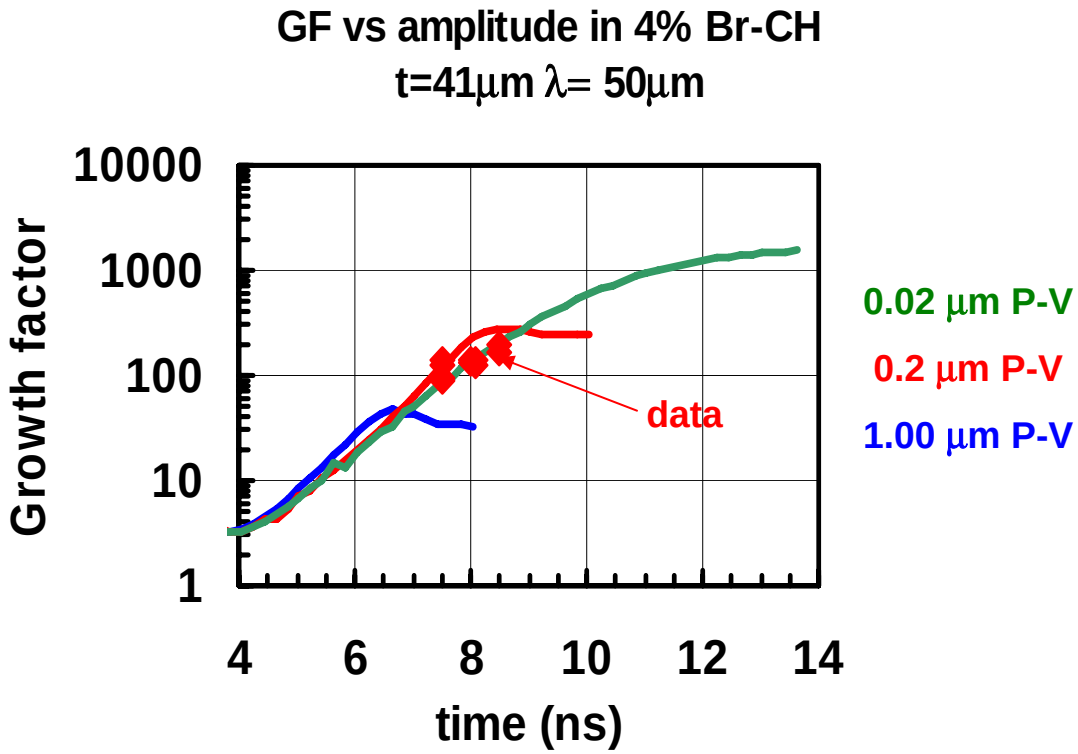
GF vs amplitude in 4% Br-CH
t=41μm λ= 50μm
Growth factor
10000
1000
100
10
1
4
6
8
10
12
14
time (ns)
data
0.02 μm P-V
0.2 μm P-V
1.00 μm P-V

Figure 5

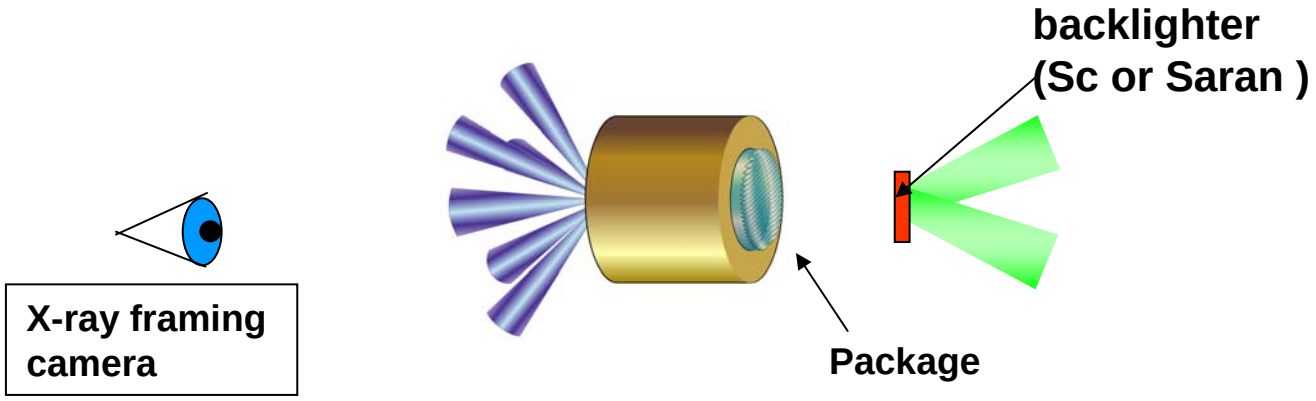

figure 6

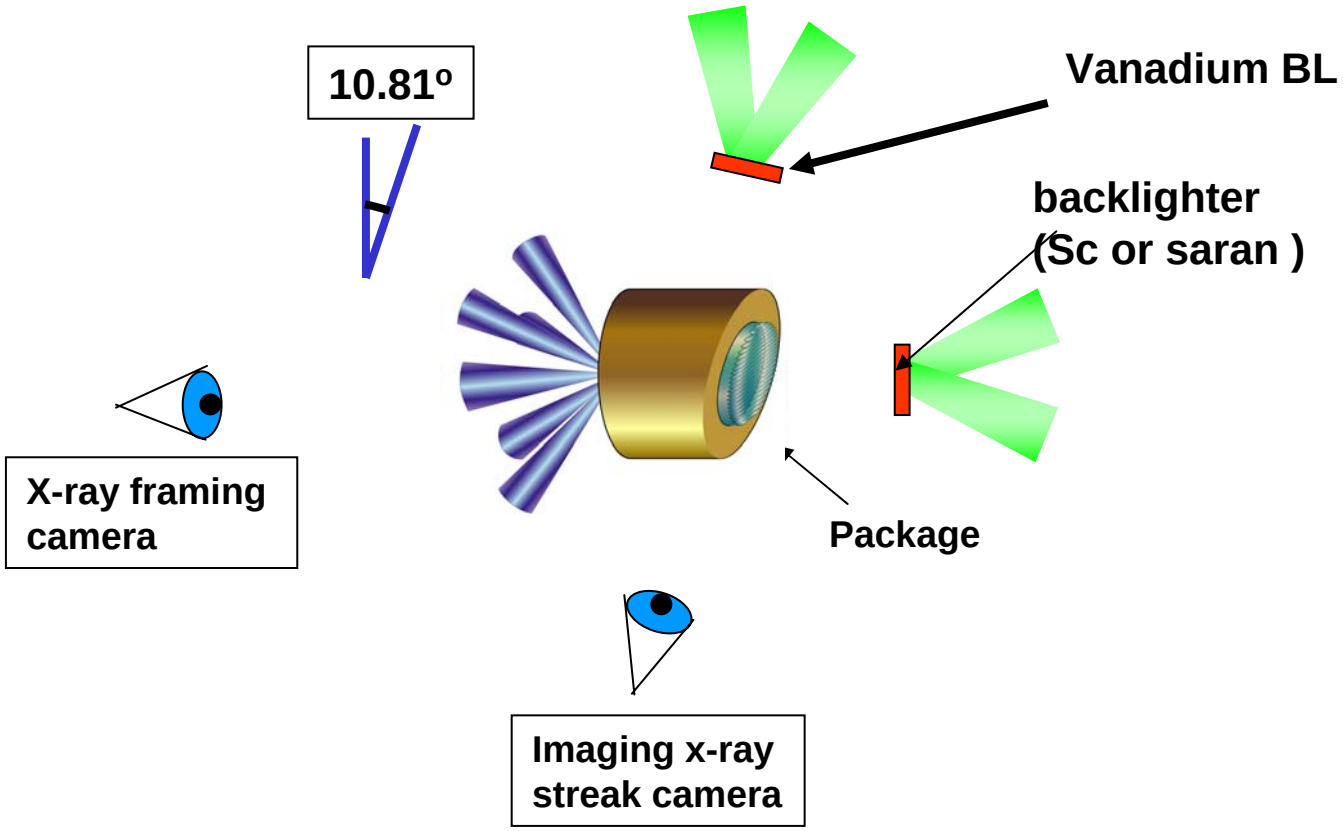
10.81º
Vanadium BL
backlighter
(Sc or saran)
X-ray framing
camera
Package
Imaging x-ray
streak camera

figure 7

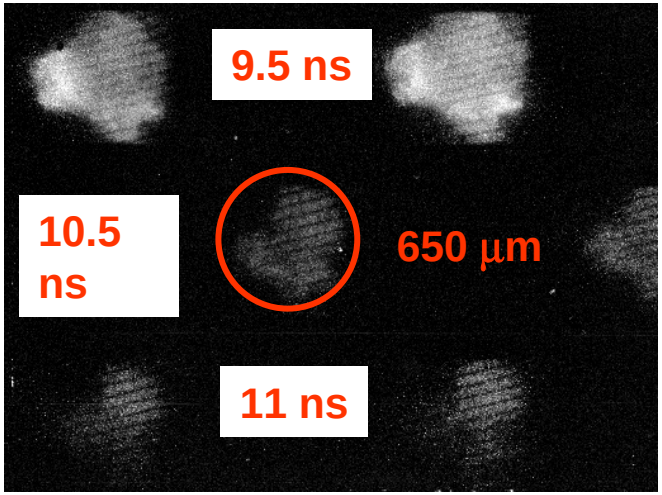

figure 8

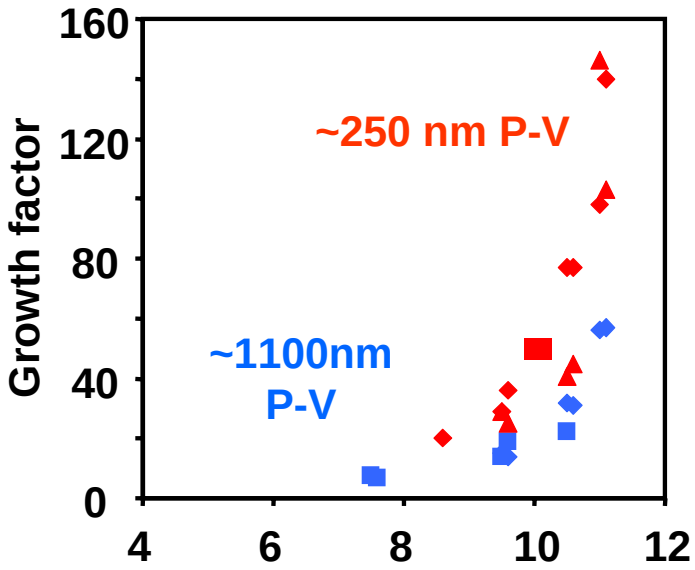

fig 9

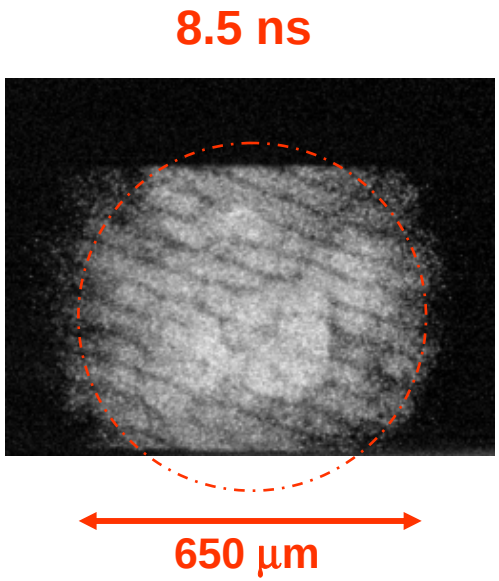

figure 10

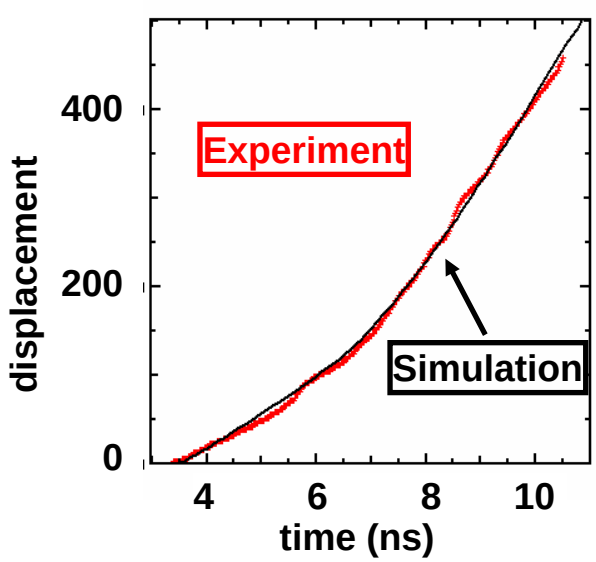
displacement
400
200
0
Experiment
Simulation
4
6
8
10
time (ns)

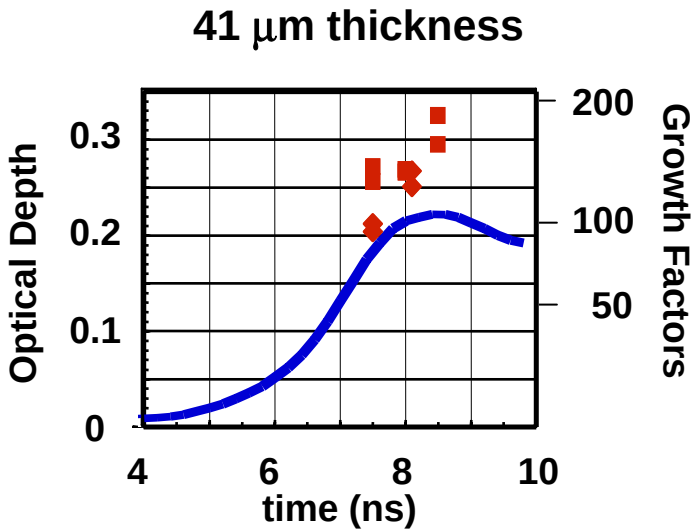
41 μm thickness
Optical Depth
0.3
0.2
0.1
0
200
100
50
Growth Factors
4
6
8
10
time (ns)

figure 11

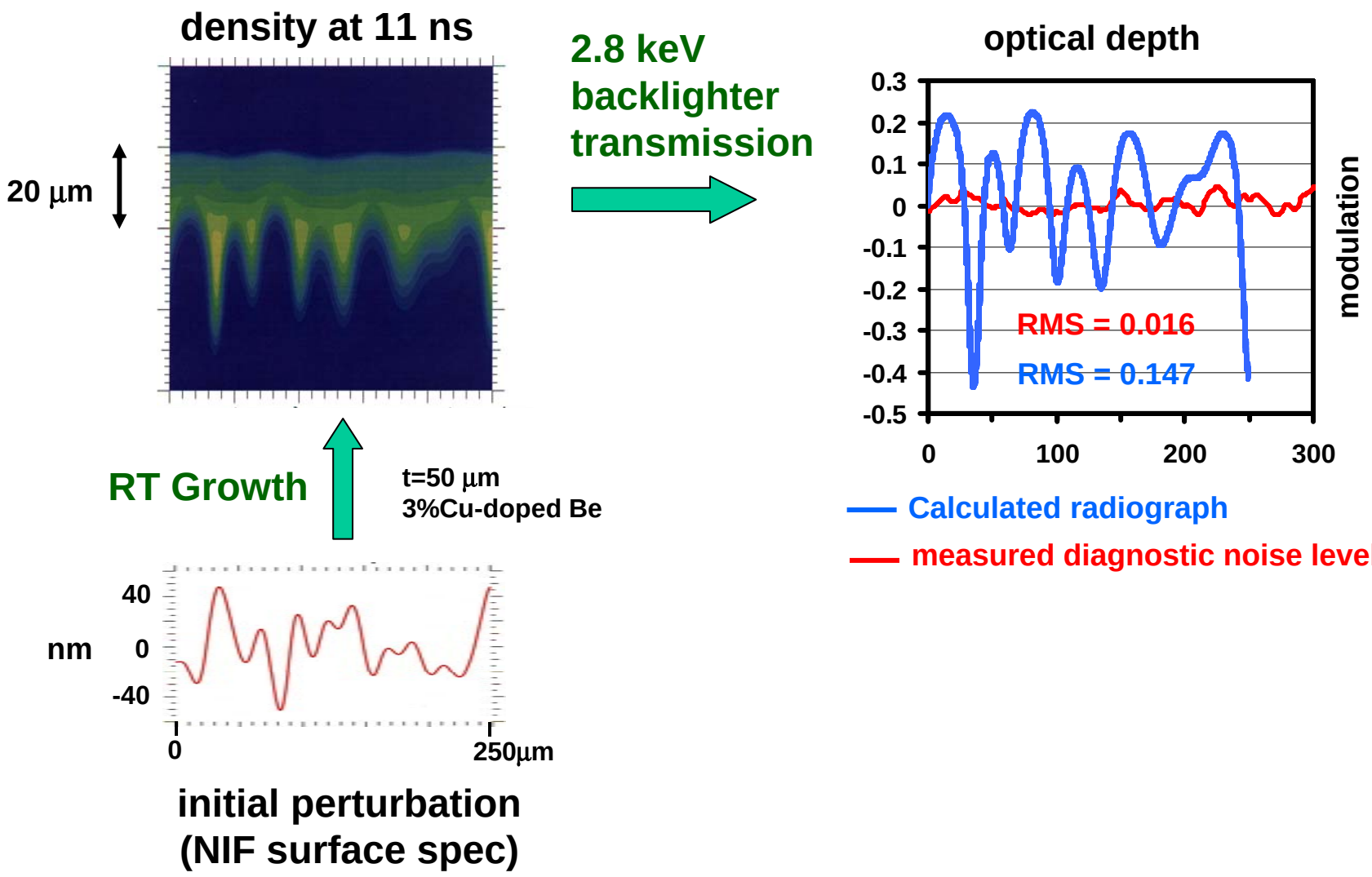
density at 11 ns
20 μm
2.8 keV
backlighter
transmission
optical depth
0.3
0.2
0.1
0
-0.1
-0.2
-0.3
-0.4
-0.5
0
100
200
300
modulation
RMS = 0.016
RMS = 0.147
Calculated radiograph
measured diagnostic noise level
RT Growth
t=50 μm
3%Cu-doped Be
40
nm 0
-40
0
250μm
initial perturbation
(NIF surface spec)

figure 12